ORIGINAL ARTICLE

Comparison of MCNPX and EGSnrc Monte Carlo Codes in the Calculation of Nano-Scaled Absorbed Doses and Secondary Electron Spectra around Clinically Relevant Nanoparticles

Asghar Mesbahi [1*], Mostafa Robatjazi [2], Hamid Reza Baghani [3], Elham Mansouri [4], Mohammad Mohammadi [5]

[1] *Radiation Oncology Department, Olivia Newton-John Cancer Wellness & Research Centre, Austin Hospital, Melbourne, Australia*

[2] *Department of Medical Physics and Radiological Sciences, Sabzevar University of Medical Sciences, Sabzevar, Iran*

[3] *Physics Department, Hakim Sabzevari University, Sabzevar, Iran*

[4] *Drug Applied Research Center, Tabriz University of Medical Sciences, Tabriz, Iran*

[5] *Department of Medical Physics, Royal Adelaide Hospital, Adelaide, Australia*

*Corresponding Author: Asghar Mesbahi
Email: amesbahi2010@gmail.com

Received: 14 March 2022 / Accepted: 25 July 2022

Abstract

Purpose: Absorbed dose enhancement due to the presence of high atomic number Nanoparticles (NP)s has been estimated and modeled by Monte Carlo (MC) simulation methods. In the current study, two MC codes of Monte Carlo N-Particle eXtended (MCNPX) and EGSnrc codes were compared by calculation of secondary electron energy spectra and nano-scaled dose values around four types of spherical NPs.

Materials and Methods: The MC model was composed of a spherical nanoparticle with a diameter of 50 nm and mono-energetic sources of photons with energies of 30,60, and 100 keV. The secondary electrons emitted from the nanoparticle were scored on the nanoparticle surface and the delivered dose to water around the nanoparticle was tallied using concentric shells with a thickness of 25 nm. Four different elements were used as materials of NPs, including Gold, Bismuth, Gadolinium, and Hafnium.

Results: Our results showed a considerable difference in the number of emitted electrons per incident photon between the two codes. There were also discrepancies between the two codes in the energy spectra of secondary electrons. Calculated radial dose values around NPs in nano-scale had a similar pattern for both codes. However, significant differences existed for some elements.

Conclusion: It can be concluded that the results of nano-scaled MC modeling for nanoparticle-based radiation therapy are dependent on the code type and its algorithm for electron transport as well as exploited cross-section libraries.

Keywords: Nanoparticle; Electron; Spectra; Monte Carlo N-Particle eXtended; EGSnrc.

DOI: https://doi.org/10.18502/fbt.v10i3.13149

Frontiers in BIOMEDICAL TECHNOLOGIES

1. Introduction

In recent years, enormous studies have been conducted to evaluate the dose sensitization effect of metallic Nanoparticles (NP)s in radiation therapy with photons [1-3]. The pioneering studies indicated a significant dose enhancement of Gold NPs in treating cancer using laboratory animals [4, 5]. The new findings motivated a large number of investigations to be performed on the application of NPs in radiation therapy. Furthermore, some researchers started to investigate the physical basis of nanoparticle-aided radiation therapy by utilizing analytical methods and Monte Carlo (MC) modeling [6, 7].

Despite a strong convergence of experimental results on the efficacy and potential of NPs in improving the outcome of radiation therapy, there is not a clear consensus on the resultant estimations of Dose Enhancement Factors (DEF) for various NPs by different mathematical models as well as theoretical studies [2, 6, 8-11]. In this regard, analytical formulas have been proposed and used for DEF calculations by several research groups for different NPs. However, the results have shown a very marked discrepancy for one nanoparticle such as Gold as well as other NPs, including Bismuth, Gadolinium, etc. [2, 9, 11-14].

Monte Carlo (MC) modeling of radial absorbed dose values and secondary electron spectra for NPs has been reported by using various types of codes such as Monte Carlo N-Particle eXtended (MCNPX), EGSnrc, FLUKA, and GEANT on micro-and nano-scale. But the published data on nano-scale, including secondary electron spectra and its resultant absorbed dose values around NPs are not comparable and large differences exist among published data [14-18]. A part of the differences in the estimated DEF and electron spectra stems from the discrepancies in electron transport algorithms and modeling approaches, including micro and nano-scales which are employed in MC codes. An inter-comparison study on different MC codes for dose enhancement estimations and secondary electron spectra revealed significant differences among studied codes [19]. The study was done on gold NPs only and no other NPs were investigated.

The type of algorithm used in MC modeling and code programming creates discrepancies in the MC estimated DEFs for NPs in the presence of low-energy photons. Moreover, these codes are used commonly in studies on the dose enhancement effect of NPs in brachytherapy with low-energy photons, because the electron transport algorithm plays a crucial role in the simulation of nanometric movements of secondary electrons and resultant DEFs. Consequently, the estimation of dose enhancement of NPs by different codes has led to different DEF values. Therefore, in the current study, we aimed to analyze the differences between two commonly used codes and address the questions in this regard. Also, we provided comparative data about NPs of Gold, Bismuth, Gadolinium, and Hafnium which were actively evaluated for radiosensitization effect in radiotherapy.

2. Materials and Methods

Two MC codes of MCNPX (version:2.7.0, Los Alamos National Laboratory, USA) [20] and EGSnrc (Stanford Linear Accelerator Center, USA) [21] were used for modeling in the current study. First, a spherical NP with a diameter of 50 nm was simulated. Then, multiple concentric spherical surfaces and shell-like cells with a thickness of 25 nm were modeled around NPs to score both secondary electron energy spectra as well as a deposited dose with distance from the nanoparticle surface. In total, 160 concentric cells were defined around an NP and dose deposition was simulated to a distance of 4 µm from the NP surface. The simulated geometry is shown in Figure 1. Monoenergetic Photon beams with a circular cross-section were used and three different energies of 30, 60, and 100 keV to irradiated the NP. The diameter of the photon source was 50 nm and parallel rays were utilized. The configuration of geometry was so

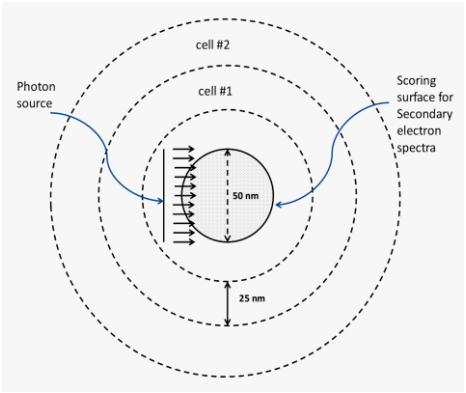

Figure 1. The simulated geometry used for secondary electron and absorbed dose determination with a spatial resolution of 25 nm irradiated by mono-energetic photons of 30, 60, and 100 keV and for nanomaterial types of Gold, Bismuth, Gadolinium, and Hafnium

to avoid other influencing effects which may originate from source complexity according to Leung *et al*. [22]. This geometry was recommended for comparison between NPs to study the secondary electron production and resultant dose deposition around an NP. The source was located at a distance of 10 nm from NP inside the first scoring cell (Figure 1). No material definition was used for the first scoring cell (the source located one) to avoid secondary electron production from this cell and only the secondary electrons of the NP were scored. The geometry, including the photon source, NP, and scoring cells was located in a water phantom with dimension of 10 × 10 × 10 cm^3 to take all possible backscattered radiation into account.

Dosimetric parameters, including energy spectra for secondary electrons and absorbed dose around a spherical nanoparticle filled with atoms of Bismuth, Gold, Gadolinium, and Hafnium were estimated. MCNPX and EGSnrc codes are capable to simulate the transportation of secondary electrons down to 1 keV energy which has a range of 10 nm in water.

The dosimetric quantities were calculated for all NPs irradiated by mono-energetic beams of 30, 60, and 100 keV to cover the energy range of mostly used brachytherapy sources such as ^{125}I, ^{103}Pd, etc. The selection of the nanoparticle types was based on previous studies, which reported potential and advantages for these NPs [13, 14, 18, 23-25]. Studied NPs consisted of Bismuth (Z = 83, density = 9.78 g/cm^3), Gold (Z = 79, density = 19.32), Gadolinium (Z = 64, density = 7.89), and Hafnium (Z = 72, Density= 13.31).

2.1. EGSnrc Code and Simulation Process

The EGSnrc Monte Carlo code is a radiation transport simulation code which is an extended and optimized version of the Electron Gamma Shower (EGS) software package that was developed at the Stanford Linear Accelerator Center (SLAC) in the 1970s.

To simulate the considered geometry using EGScpp (a geometry definition module), at the first step, the "egs_spheres library" was used. Different library of "Ausgabe" definition such as "egs_dose_scoring", "egs_phsp_source" was used in different steps of the simulation process. The "egs_phsp_source library" was used to score produced secondary electrons in a phase-space on the surface of NPs. Then, this phase-space was used as a source in the calculation of dose values in the considered scoring shells using "egs_dose_scoring library". To obtain the particle spectra, the phase-space is imported to the Beamdp code and the electron spectra are extracted from each phase-space. The PRESTA-II was utilized as the cross-section data and electron transport algorithm, respectively, in the simulation process. The PRESTA-II is based on the class-II of the Condensed History Scheme (CHS), a more accurate algorithm than the previous version of this algorithm (PRESTA-I), in which correlation between secondary and primary particles was considered. The energy cut-off values for electrons and photons (ECUT and PCUT) as well as AE, and PE (The production by electrons of secondary particles with kinetic energy greater than these values is modeled explicitly) were considered equal to 1 keV. The primary photon history used in each simulation process was considered equal to 109, so that, the statistical uncertainty of obtained values was below 1%.

2.2. MCNPX Code and Simulation Process

In the current study, MCNPX (2.7.0) with the updated ENDF/B-VIII data library was used for particle transport and interactions with the considered media. The class-I CHS was employed in the electron transport algorithm of this code [26]. The employed electron and photon interaction cross-sections were El03 and mcplib04 data libraries, respectively. To score the secondary electrons, including photoelectrons and auger electrons, energy spectra were tallied using the F2 scoring tally. This tally scored the number of electrons reaching a surface (number per cm^2) for all concentric planes starting from the radius range of 50- 4000 nm with an increment of 25 nm. Also, the deposited dose in the peripheral was scored using *F8:e scoring tally and the dose components of primary and scattered photons were excluded by setting the importance of photons to zero for all scoring cells.

3. Results

The radial dose calculations in a nanometric scale for four NPs and mono-energetic photon beams of 30, 60, and 100 keV are illustrated in Figures 2-4. Overall, the calculated absorbed doses by the MCNPX code are higher than those estimated by the EGSnrc code at the same distance from NPs. Besides, these differences in the scored doses by two MC codes increments with an increase in the initial photon energy, and the highest gap between codes were seen in 100 keV photons.

In Figure 2, the results were presented for 30 keV photon energy. It can be seen from Figures 2a and b, that the calculated absorbed dose curves by two codes indicate a relatively fair match for gold and bismuth NPs, while for gadolinium and hafnium (Figure 2c and d) the degree of superimposition and similarity in pattern diminishes. To be more precise, in the cases of gadolinium and hafnium, estimations by MCNPX are approximately two times higher than those of EGSnrc in a distance of 1000 - 4000 nm from the NP surface.

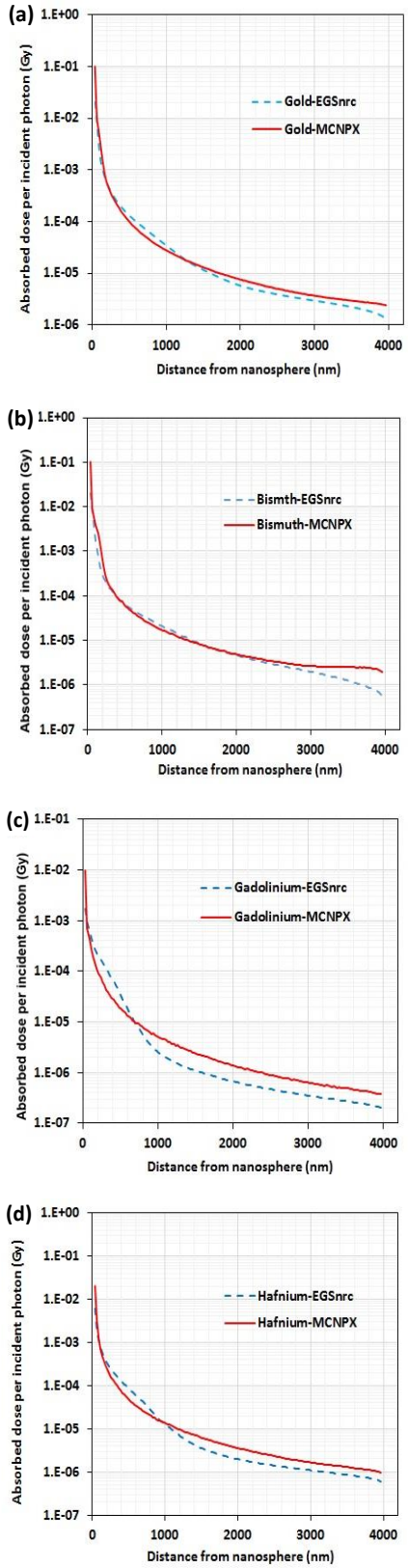

Figure 2. The calculated absorbed dose per incident primary photon with the energy of 30 keV. (a) Gold (b) Bismuth (c) Gadolinium (d) Hafnium

The variation of absorbed dose with distance from the NP surface for 60 keV photon beam was shown in Figure 3. In Figures 3a, b like in the case of 30 keV photons, there are close estimations between two codes for both gold and bismuth NPs. However, for gold, EGSnrc estimated higher doses relative to MCNPX up to 1400 nm and then the values of MCNPX were more than EGSnrc estimations. For bismuth NP, the same pattern was seen where the intersection of two curves is located at a distance of 1600 nm from the NP surface. In Figure 3c, the calculated doses for gadolinium by MCNPX code were two times higher compared to EGSnrc calculations. For hafnium NP, as it is shown in Figure 3d, the dose variation with distance is very similar to gold and bismuth NPs but the intersection of two curves occurs at a distance of 1000 nm from the NP surface.

In Figure 4, the estimations of absorbed dose with distance by two codes are illustrated for 100 keV photons. It is clearly shown that the MCNPX code overestimates the absorbed dose with distance for all studied NPs. There are approximate superimpositions between two codes in all NPs over a distance of about 500 nm. After that, the MCNPX overestimates the absorbed dose compared to the EGSnrc. The biggest difference between the two codes happens in a distance of 2000 - 3000 nm for gold, while for bismuth NP it occurs in a distance of 3000 - 4000 nm. Clearly visible differences are observed between the two codes in a distance of 600 - 1400 nm and 1400 - 2400 nm for gadolinium and hafnium NPs, respectively.

The secondary electron energy spectra for gold, bismuth, gadolinium, and hafnium NPs irradiated by mono-energetic photon beams of 30, 60, and 100 keV are shown in Figures 5-7. These spectra are composed of photoelectrons coming from different shells and sub-shells such as K, L, and M electronic layers which make the peaks in their corresponding energy for each NP. There are also low energy (<10 keV) Auger and Coster-Kronig electrons with low penetration which deposit their energy in the proximity of the NP surface.

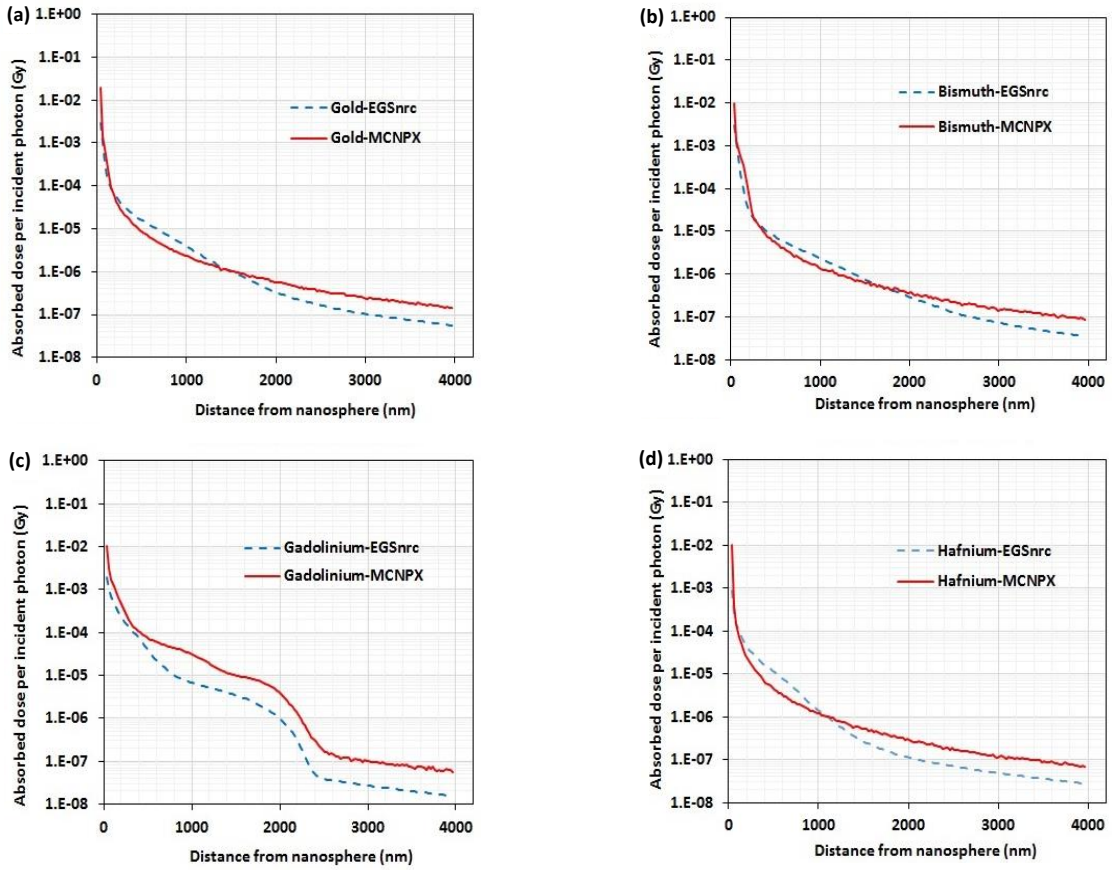

Figure 3. The calculated absorbed dose per incident primary photon with the energy of 60 keV. (a) Gold (b) Bismuth (c) Gadolinium (d) Hafnium

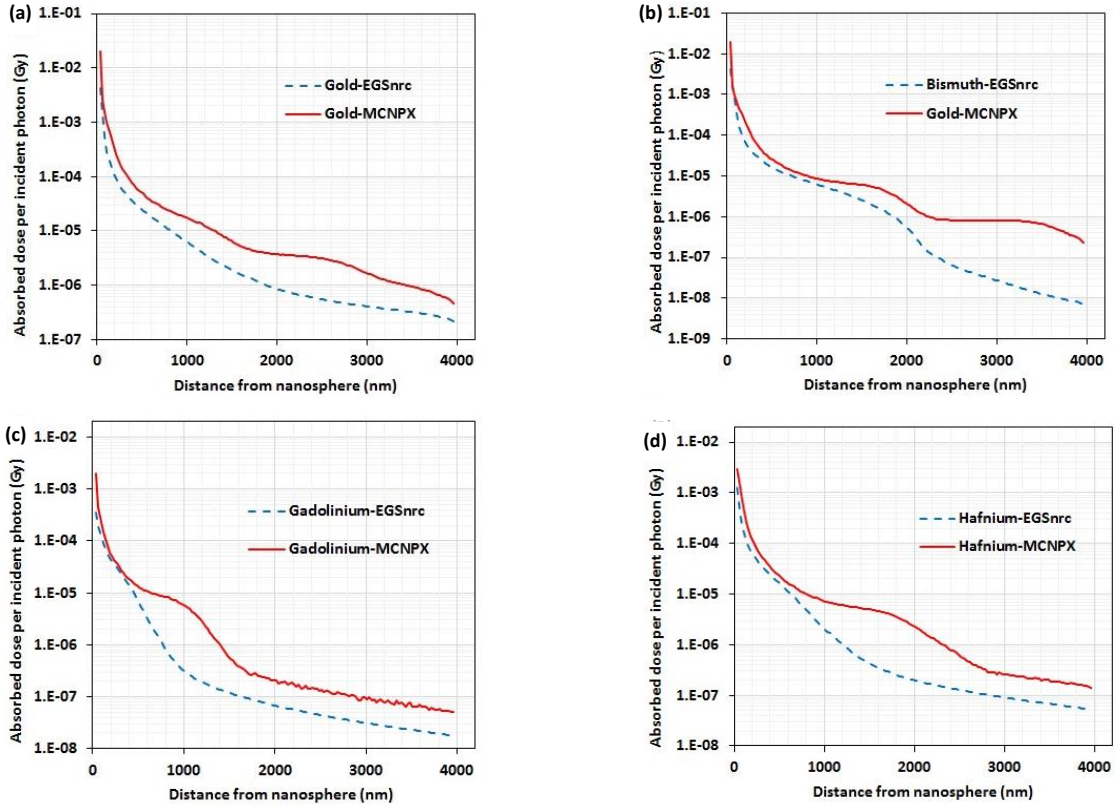

Figure 4. The calculated absorbed dose per incident primary photon with the energy of 100 keV. (a) Gold (b) Bismuth (c) Gadolinium (d) Hafnium

In Figure 5, the simulated results of MCNPX and EGSnrc codes for electron energy spectra are depicted for 30 keV photons. For gold NP, the number of secondary electrons calculated by EGSnrc in the energy range of 4 - 15 keV is 100 times higher than those of the MCNPX code (Figure 5a). A similar pattern exists for all other NPs but the gaps between the two codes occur in different energy ranges for studied NPs. Precisely speaking, the gaps between the two codes are apparent in the energy ranges of 5 - 14, 4 - 7, and 4 - 10 keV for bismuth, gadolinium, and hafnium, respectively. Furthermore, there are several peaks in the calculated spectra for all NPs. The peaks of photoelectrons emitted from L and M shells were identified by PEL and PEM on all figures. There is excellent conformity between the two codes in demonstrating the photopeaks for all NPs. However, EGSnrc is capable to simulate photopeaks of sublayers for L and M shells while MCNPX exhibits only one photopeak for each shell, including M and L. It is attributed to the modeling features of MCNPX and EGSnrc codes. For instance, the peaks of L-1, L-2, and L-3 sublayers are shown separately in Figure 5 for all NPs, while MCNPX shows only one peak for all L sublayers.

In Figure 6, electron spectra for 60 keV photons are displayed. There is a good agreement between photopeaks of both codes in all NPs. On the other hand, there are several differences in the number of secondary electrons estimated by the two codes. For all NPs, the differences in electron fluence with energy less than 10 keV are associated with the overestimation of the EGSnrc code. In Figure 6b which shows the electron spectra for bismuth NP, a gap between two spectra is seen in the energy range of 6-16 keV and EGSnrc overestimation reaches up to 10 times relative to MCNPX. For gadolinium, (Figure 6c) gaps are seen in electron fluence between 12 - 20 keV and 34 - 50 keV energy ranges.

Figure 7 illustrates the electron energy spectra for 100 keV photons impinged on gold, bismuth, gadolinium, and hafnium NPs. The agreement between two codes in the identification of photopeaks of K, L, and M layers is evident. In this energy, the photopeaks of the K layer are seen in all NPs and marked with PEK in the figures. For all NPs, the values of EGSnrc are significantly higher than the values of the MCNPX code. There are marked disparities in the number of electrons from 28 to 36 keV for gold and bismuth NPs (Figure 7a, b). There are also other gaps between the two codes for gold (60-88 keV) and bismuth (70 - 82 keV). In Figure 7c, d which shows the emitted electrons from the gadolinium and hafnium NPs, the conformity between photopeaks is apparent, but for hafnium NP, MCNPX estimations are higher than those of EGSnrc for electrons less than 30 keV.

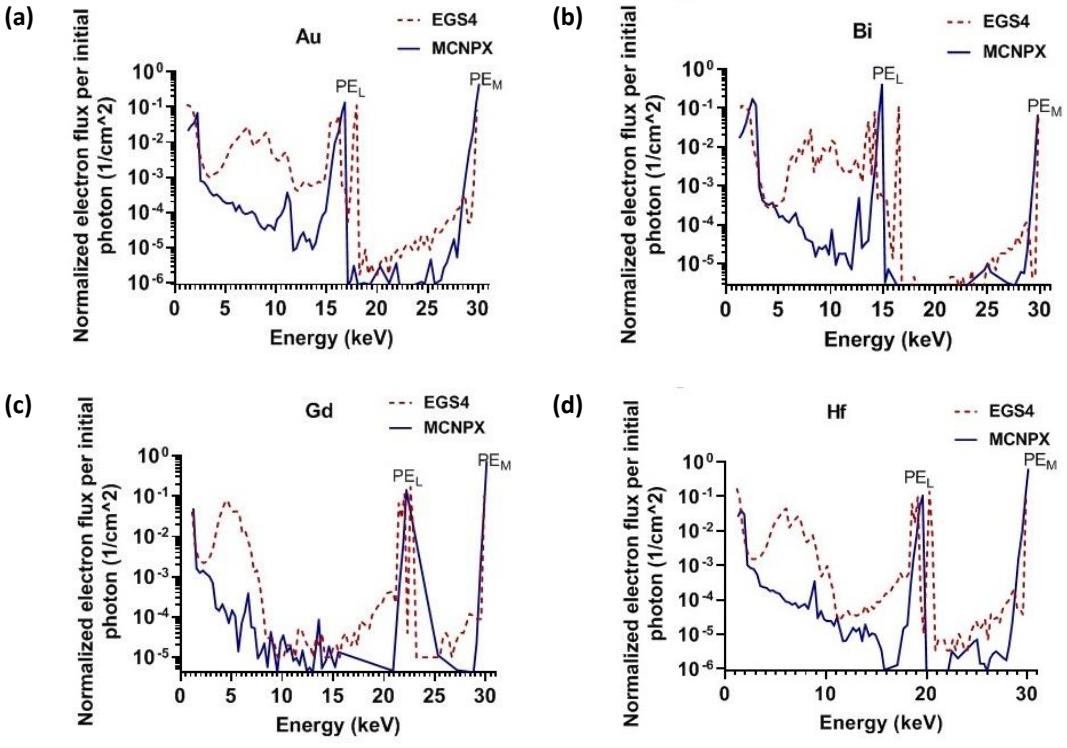

Figure 5. The calculated electron energy spectra by two MC codes from a nanosphere with a diameter of 50 nm irradiated by mono-energetic 30 keV photons. (a) Gold (b) bismuth (c) Gadolinium (d) Hafnium

Overall, noticeable discrepancies can be seen between MCNPX and EGSnrc codes. For photoelectrons coming from K- and L edges, there are proper superimpositions between MCNPX and EGSnrc for all NPs and photon energies. EGSnrc code provides more detailed information on photopeaks compared to MCNPX. Moreover, it can be deduced from all provided data in the current study that the number of secondary electrons scored by the EGSnrc is on average 1440 times higher than those estimated by MCNPX.

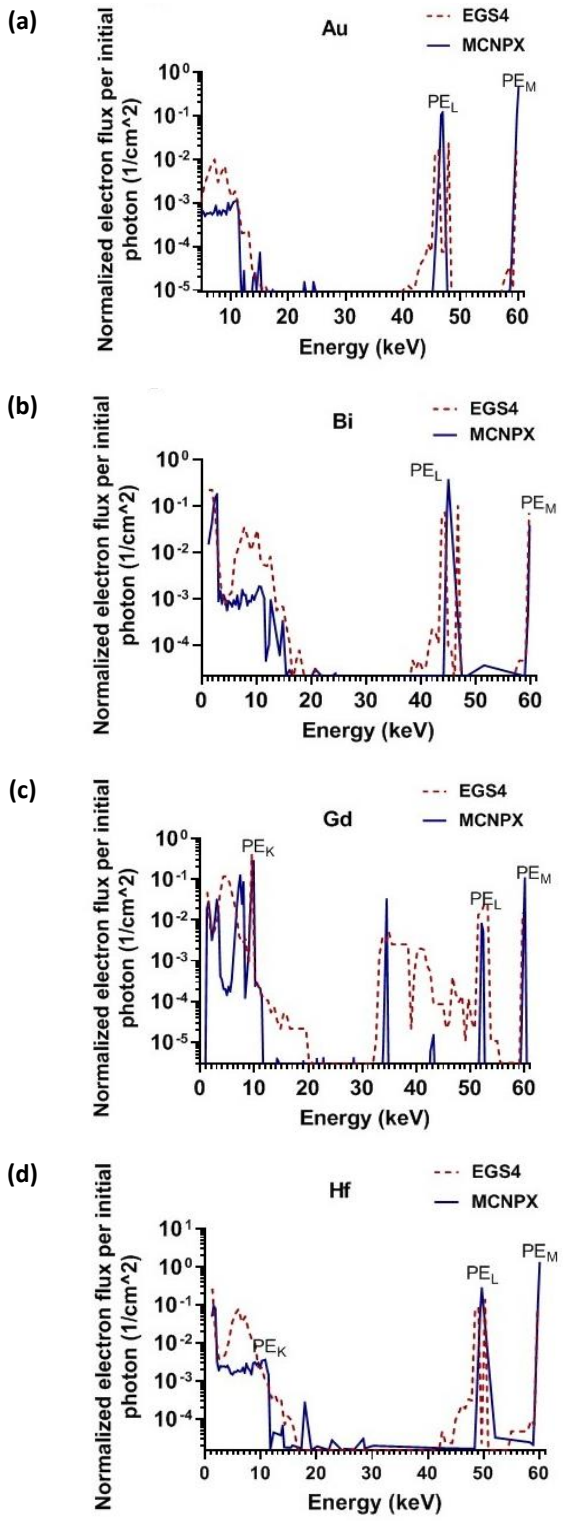

Figure 6. The calculated electron energy spectra by two MC codes from a nanosphere with a diameter of 50 nm irradiated by mono-energetic 60 keV photons. (a) Gold (b) bismuth (c) Gadolinium (d) Hafnium

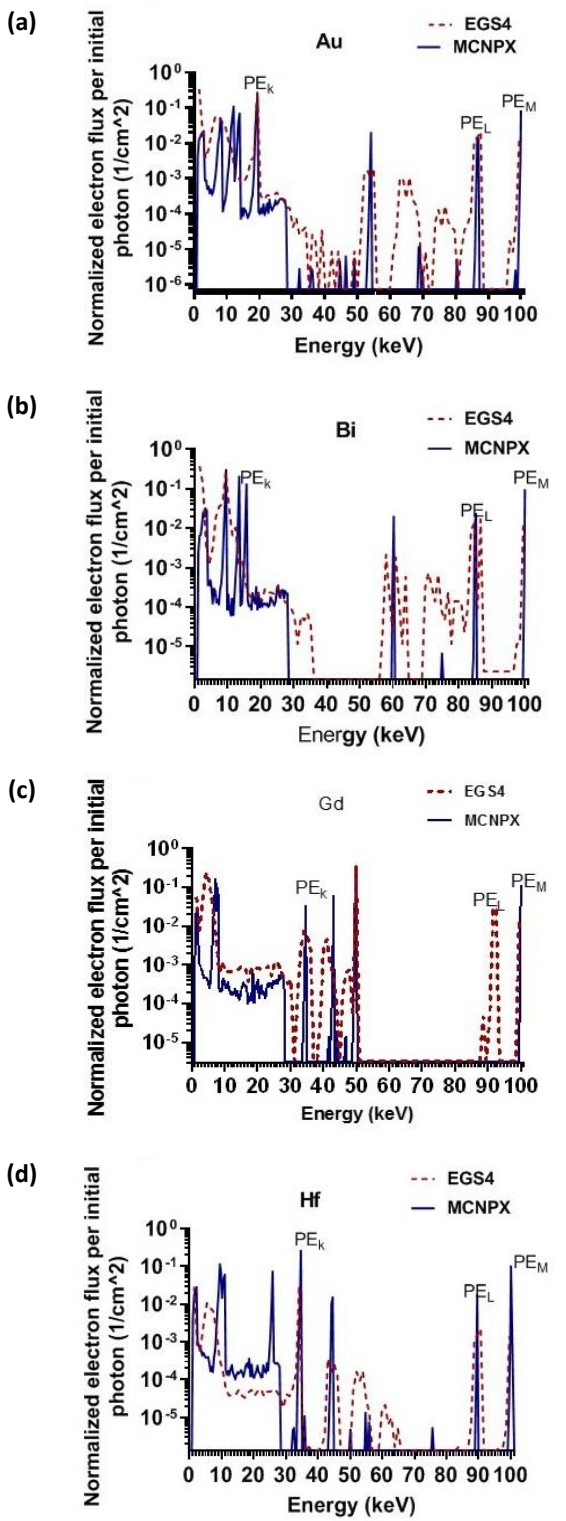

Figure 7. The calculated electron energy spectra by two MC codes from a nanosphere with a diameter of 50 nm irradiated by mono-energetic 100 keV photons. (a) Gold (b) bismuth (c) Gadolinium (d) Hafnium

4. Discussion

In the present study, we calculated the radial absorbed dose and electron energy spectra of secondary electrons around spherical NPs. Our results indicated some similarities in the fall-off of absorbed dose with distance and electron spectra between two MC codes of MCNPX and EGSnrc. However, there are some disparities between the two codes and also differences among studied NPs.

For radial dose calculations, the results of both codes indicated an exponential dose fall-off by distance from NPs and it was in agreement with previous studies on gold and gadolinium NPs [13, 24, 27-29]. The gold and bismuth NPs had comparable radial dose values in all energies. On the other hand, as it was expected, hafnium and gadolinium showed reduced doses relative to gold and bismuth NPs due to their lower atomic number. The radial doses for all NPs depend strongly on the secondary electron energy spectra and the number of produced electrons per initial photon. Moreover, the atomic number of a nanoparticle determines its atomic structure and electronic shells around the nucleus. Also, the electrons binding energies of K, L, and M shells vary considerably with the atomic number which plays a critical role in the probability of photoelectric interactions of photons with binding electrons. Consequently, incident photon energy and the atomic number of nanoparticles are very influencing parameters in secondary electron production and spectra. The maximum probability for secondary electron production occurs when the photon energy becomes higher than the K, L, and M binding energies. For instance, at 60 keV, when the energy of photons exceeds the k-electron binding energies of the gadolinium atom (K-edge, 50.2 keV), photoelectron production increases and causes a higher radial dose around the NP. Our findings were in line with the results of Sherck *et al.* who simulated gold, calcium tungstate, and hafnium oxide NPs to evaluate their dose enhancement in radiation therapy [25]. Their results indicated that based on the atomic number of NPs, radial dose and secondary electron fluence for Gold (Z = 79) were higher calcium tungstate (Ztungsten = 74, and hafnium oxide (Zhafnium = 72) NPs in monoenergetic photon energy of 160 keV. They attributed the close values between the tungsten and hafnium NPs to their similar electronic structures.

The shape of radial dose around the NPs is affected strongly by the electron spectra because the range of electrons and their energy deposition in terms of KeV/mm around the NPs are completely dependent on their energies. Thus, with the increase in primary photon beam and secondary electron energies, the pattern of dose deposition varies significantly for each NP (Figures 2-4). Consequently, the radial dose values with approximate exponential decline have shown variable patterns for studied photon energies and NPs. Another point worth mentioning is that the difference between the two codes became bigger with photon energies. It is greatly attributed to the distinct methods used for electron transportation by codes. The shape of absorbed dose-distance curves for gold and bismuth NPs (30 and 60 keV) were very close to the conducted study on gold NP by Villagomez-Bernabe and Currel [17]. They illustrated a monotonically decreasing energy deposition with distance from the nanoparticle. However, the small fluctuations were related to the energies of emitted electrons and their corresponding ranges in water.

We also calculated the secondary electron energy spectra for the studied NPs using two different codes. As it can be seen in Figures 5-7, considerable fluctuations exist for electron fluence in all studied energies for both codes which could be attributed to the statistical nature of electron transport algorithms used by the two different codes. A considerable disparity was found in the secondary electron production rate per incident photon between the two codes. We think that the main reason for these discrepancies is the difference between the considered CHS employed by each code during the electron transport simulation. In this regard, the EGSnrc uses class-II CHS (known as PRESTA-II in EGSnrc), while the class-I CHS is employed by the MCNPX MC code. The most remarkable difference between class-I and class-II CHS is the considered approach in treating the secondary particles which are created following the individual electron interactions. In class-II CHS, a threshold energy is considered for produced secondary particles, including bremsstrahlung photons and delta rays. If the energy of produced secondary particles were lower than this threshold energy, the effects of secondary particles grouped during each step of electron path simulation and none of these secondary particles would be individually transported. In return, if the secondary particle energy exceeds the considered threshold energy, each produced secondary particle is treated as an individual particle and would be separately transported. In contrast, in class-I CHS, the effects of created secondary particles during the initial electron interactions are always grouped regardless

of their corresponding energy. Therefore, it can be concluded that the number of secondary electrons that are produced following the class-II CHS would be higher and as a consequence, the number of scored secondary electrons emitted from the surface of NPs would be increased. In the study of Lashkari *et al.*, both MCNPX and EGSnrc codes were used to calculate the dosimetric characteristics of a radiation therapy beam [19]. The results were compared to the measurements. Although the results of both codes were comparable, they reported a superior accuracy for EGSnrc calculations. Our findings are in close agreement with their results concerning the differences observed between MCNPX and EGSnrc codes in dose calculations and electron-photon simulation algorithms.

The observed deviation between calculated dose values can be also linked to the employed CHS by two studied MC codes during the electron transport simulation. As mentioned previously, MCNPX uses the class-I CHS, while the EGSnrc employs the class-II CHS. In class-I CHS the effects of secondary particles, including bremsstrahlung photons and delta rays are grouped during each electron step simulation. This means that the energy of these secondary particles would be locally deposited and no subsequent individual transport would be considered for such low-energy particles. Consequently, it can be deduced that the deposited energy inside each scoring shell would be increased. On the other hand, the EGSnrc code employs the class-II CHS for electron transport simulation through which each secondary particle can be treated as an individual one and separately transported (if its energy were higher than the predefined threshold energy). As a result, the energy of these secondary particles may not be locally deposited within a certain scoring shell and instead, would be distributed between some consecutive scoring shells. This process can finally reduce the scored dose in each scoring shell concerning the local energy deposition of created secondary particles, which is considered in class-I CHS. Therefore, it can be expected that the MCNPX code results would be higher absorbed doses in comparison with the EGSnrc code.

We only found one published paper that compared several MC codes on a gold nanoparticle in the same irradiation geometry by Li *et al.* and large uncertainties up to 2.3 in calculated DEF were reported among studied MC codes [11]. Our results are in agreement with their findings which emphasize the shortcoming of different MC codes in accurately modeling electron transportation in nano-scaled and dose deposition calculations. The geometry used in this study was only used for the comparison of different NPs in terms of atomic number and secondary electron emissions [22, 28, 30]. In the clinical or experimental studies, the irradiation geometries are very different from our used case, where isotropic or divergent beams, as well as polychromatic photon beams, are employed for NP-aided treatments. Thus, the results of the current study cannot be generalized for real treatment geometries. Also, a nanometric scale used for dose deposition could result in overestimation or underestimation of dose enhancement factors in this regard.

It is worth mentioning that there is no experimental data on the actual values of the calculated quantities, including secondary electron energy spectra, nano-scaled dose deposition, and its resultant DEF. Consequently, in our MC study and all similar MC-based investigations on NPs and their related dosimetric quantities, it would be impossible to determine the most accurate and reliable MC code and results. Nevertheless, it can be said that more computational and modeling improvements are required to result in higher convergence of MC calculations by different codes, especially in the case of nanoparticle-related calculations.

5. Conclusion

In the present study, we simulated the secondary electron spectra and absorbed dose in nanoscale for different NPs and photon energies using EGSnrc and MCNPX MC codes. The obtained results showed that there are remarkable discrepancies in calculated secondary electron energy spectra and dose values. Such observed deviations between the Monte Carlo results can be mainly attributed to the employed electron transport simulation algorithms which are used by the considered MC codes. Owing to the fact that EGSnrc code provides more detailed histories during the simulation of each electron step, it can be concluded that the calculated dose values and secondary electron energy spectra by EGSnrc MC code have more precision on the nanoscale.

References

1- R. Ahmad *et al.*, "Radiobiological Implications of Nanoparticles Following Radiation Treatment." Presented at the Part. Part. Syst. Charact

Particle and Particle Systems Characterization, 2020, (2020). [Online]. Available: https://www.scopus.com/inward/record.uri?eid=2-s2.0-85081038632&doi=10.1002%2fppsc.201900411&partnerID=40&md5=830636d0a98a4336d079a21c4fb343e2.

2- R. Delorme *et al.*, "Comparison of gadolinium nanoparticles and molecular contrast agents for radiation therapy-enhancement." Presented at the *Med. Phys*

Medical Physics, 2017, (2017). [Online]. Available: https://www.scopus.com/inward/record.uri?eid=2-s2.0-85031409637&doi=10.1002%2fmp.12570&partnerID=40&md5=8101dc0dd6bd3addc51fd214c8054af6.

3- J.F. Hainfeld, F.A. Dilmanian, D.N. Slatkin, and H.M. Smilowitz, "Radiotherapy enhancement with gold nanoparticles." *J. Pharm. Pharmacol*, Vol. 60 (No. 8), pp. 977-85, 8/2008 (2008).

4- J.F. Hainfeld, D.N. Slatkin, and H.M. Smilowitz, "The use of gold nanoparticles to enhance radiotherapy in mice." *Phys. Med. Biol*, Vol. 49 (No. 18), pp. N309-N15, 9/21/2004 (2004).

5- W. Roa *et al.*, "Gold nanoparticle sensitize radiotherapy of prostate cancer cells by regulation of the cell cycle." *Nanotechnology*, Vol. 20 (No. 37), pp. 375101-4484/20, 9/16/2009 (2009).

6- J.D. Carter, N.N. Cheng, Y. Qu, G.D. Suarez, and T. Guo, "Nanoscale energy deposition by X-ray absorbing nanostructures." Presented at the *J Phys Chem B*

Journal of Physical Chemistry B, 2007, (2007). [Online]. Available: https://www.scopus.com/inward/record.uri?eid=2-s2.0-35548987636&doi=10.1021%2fjp075253u&partnerID=40&md5=f3d3addd90846e298aa482bbcf8e0d5a.

7- S.J. McMahon *et al.*, "Biological consequences of nanoscale energy deposition near irradiated heavy atom nanoparticles." *Sci. Rep*, Vol. 1:18p. 18, 2011 (2011).

8- M. Douglass, E. Bezak, and S. Penfold, "Monte Carlo investigation of the increased radiation deposition due to gold nanoparticles using kilovoltage and megavoltage photons in a 3D randomized cell model." *Med. Phys*, Vol. 40 (No. 7), p. 071710, 7/2013 (2013).

9- A.G. Jangjoo, H. Ghiasi, and A. Mesbahi, "A Monte Carlo study on the radio-sensitization effect of gold nanoparticles in brachytherapy of prostate by 103Pd seeds." Presented at the *Pol. J. Med. Phys. Eng*

Polish Journal of Medical Physics and Engineering, 2019, (2019). [Online]. Available: https://www.scopus.com/inward/record.uri?eid=2-s2.0-85068103631&doi=10.2478%2fpjmpe-2019-0012&partnerID=40&md5=fda6cba1bd2fba0729c8dfdb01d5610c.

10- A. Khodadadi, H.A. Nedaie, M. Sadeghi, M.R. Ghassemi, A. Mesbahi, and N. Banaee, "Determination of the dose enhancement exclusively in tumor tissue due to the presence of GNPs." Presented at the *Appl. Radiat. Isot*

Applied Radiation and Isotopes, 2019, (2019). [Online]. Available: https://www.scopus.com/inward/record.uri?eid=2-s2.0-85058707751&doi=10.1016%2fj.apradiso.2018.11.013&partnerID=40&md5=0171eaaf0fd4057e1cd8f4269e44006c.

11- W.B. Li *et al.*, "Intercomparison of dose enhancement ratio and secondary electron spectra for gold nanoparticles irradiated by X-rays calculated using multiple Monte Carlo simulation codes." *Physica Medica*, Vol. 69pp. 147-63, 2020 (2020).

12- L. Maggiorella *et al.*, "Nanoscale radiotherapy with hafnium oxide nanoparticles." Presented at the *Future Oncol*

Future Oncology, 2012, (2012). [Online]. Available: https://www.scopus.com/inward/record.uri?eid=2-s2.0-84867095663&doi=10.2217%2ffon.12.96&partnerID=40&md5=fd2fa110390c4407ebbf5225f2cf7df6.

13- A. Rajaee *et al.*, "Multifunction bismuth gadolinium oxide nanoparticles as radiosensitizer in radiation therapy and imaging." Presented at the *Phys. Med. Biol*

Physics in Medicine and Biology, 2019, (2019). [Online]. Available: https://www.scopus.com/inward/record.uri?eid=2-s2.0-85072944316&doi=10.1088%2f1361-6560%2fab2154&partnerID=40&md5=e6d11442b331b1a953833401e3cecd3e.

14- J.C. Roeske, L. Nu+¦ez, M. Hoggarth, E. Labay, and R.R. Weichselbaum, "Characterization of the theorectical radiation dose enhancement from nanoparticles." Presented at the *Technol. Cancer Res. Treat*

Technology in Cancer Research and Treatment, 2007, (2007). [Online]. Available: https://www.scopus.com/inward/record.uri?eid=2-s2.0-35348998981&doi=10.1177%2f153303460700600504&partnerID=40&md5=ed9f1190aeeac264df733bf0f854e48a.

15- C. Park, S. Asadi, and J.K. Kim, "Monte Carlo Simulation of Gold Nanoparticle-Enhanced Radiation Therapy." Presented at the *Eur. Cells and Mater*

European Cells and Materials, 2010, (2010). [Online]. Available: https://www.scopus.com/inward/record.uri?eid=2-s2.0-84860909116&partnerID=40&md5=63d927893716cf5c3dcbb31c28ac2749.

16- A.D. Paro, M. Hossain, T.J. Webster, and M. Su, "Monte Carlo and analytic simulations in nanoparticle-enhanced radiation therapy." Presented at the *Int. J. Nanomed*

International Journal of Nanomedicine, 2016, (2016). [Online]. Available: https://www.scopus.com/inward/record.uri?eid=2-s2.0-84988892853&doi=10.2147%2fIJN.S107624&partnerID=40&md5=24a25ef5bff838a37bd87361fff41140.

17- B. Villagomez-Bernabe and F.J. Currell, "Physical Radiation Enhancement Effects Around Clinically Relevant Clusters of Nanoagents in Biological Systems." Presented at the *Sci. Rep*

Scientific Reports, 2019, (2019). [Online]. Available: https://www.scopus.com/inward/record.uri?eid=2-s2.0-85066488973&doi=10.1038%2fs41598-019-44482-y&partnerID=40&md5=c9a37c1bfbebf2cf14ca40b1e6ac9d2f.

18- A.S. Wozny *et al.*, "Gadolinium-based nanoparticles as sensitizing agents to carbon ions in head and neck tumor cells." Presented at the *Nanomed. Nanotechnol. Biol. Med*

Nanomedicine: Nanotechnology, Biology, and Medicine, 2017, (2017). [Online]. Available: https://www.scopus.com/inward/record.uri?eid=2-s2.0-85029414907&doi=10.1016%2fj.nano.2017.07.015&partnerID=40&md5=6b2f733f1e7cd0384faa4047638bd601.

19- Sara Lashkari, Hamid Reza Baghani, Mohammad Bagher Tavakoli, and Seyed Rabi Mahdavi, "An inter-comparison between accuracy of EGSnrc and MCNPX Monte Carlo codes in dosimetric characterization of intraoperative electron beam." *Computers in Biology and Medicine*, Vol. 128p. 104113, 2021 (2021).

20- D.B. Pelowitz, "MCNPX User's Manual. Version 2.7.0, Los Alamos National Laboratory, LA-CP-11-00438.," ed, (2011).

21- I. Kawrakow, E. Mainegra-Hing, DWO Rogers, Tessier, F., and BRB Walters, "The EGSnrc Code System: Monte Carlo simulation of electron and photon transport.

Technical Report PIRS-701, National Research Council Canada .", ed, (2017).

22- M.K. Leung, J.C.L. Chow, B.D. Chithrani, M.J.G. Lee, B. Oms, and D.A. Jaffray, "Irradiation of gold nanoparticles by x-rays: Monte Carlo simulation of dose enhancements and the spatial properties of the secondary electrons production." Presented at the *Med. Phys*

Medical Physics, 2011, (2011). [Online]. Available: https://www.scopus.com/inward/record.uri?eid=2-s2.0-79551667662&doi=10.1118%2f1.3539623&partnerID=40&md5=ba76273aff2b572f491c4e8670458390.

23- C. Verry, E. Porcel, C. Chargari, C. Rodriguez-Lafrasse, and J. Balosso, "Use of nanoparticles as radiosensitizing agents in radiotherapy: State of play." Presented at the *Cancer Radiother*

Cancer/Radiotherapie, 2019, (2019). [Online]. Available: https://www.scopus.com/inward/record.uri?eid=2-s2.0-85072229624&doi=10.1016%2fj.canrad.2019.07.134&partnerID=40&md5=4725d7c0ec5c48dd74bb13408248b9a3.

24- F. Taupin *et al.*, "Gadolinium nanoparticles and contrast agent as radiation sensitizers." *Phys. Med. Biol*, Vol. 60 (No. 11), pp. 4449-64, 6/7/2015 (2015).

25- N.J. Sherck and Y.Y. Won, "Technical Note: A simulation study on the feasibility of radiotherapy dose enhancement with calcium tungstate and hafnium oxide nano- and microparticles." *Med. Phys*, Vol. 44 (No. 12), pp. 6583-88, 12/2017 (2017).

26- Stephen M. Seltzer, "Electron-photon Monte Carlo calculations: The ETRAN code." *International Journal of Radiation Applications and Instrumentation. Part A. Applied Radiation and Isotopes*, Vol. 42 (No. 10), pp. 917-41, 1991 (1991).

27- R. Casta, J.P. Champeaux, P. Moretto-Capelle, M. Sence, and P. Cafarelli, "Electron and photon emissions from gold nanoparticles irradiated by X-ray photons." Presented at the *J. Nanopart. Res*

Journal of Nanoparticle Research, 2015, (2015). [Online]. Available: https://www.scopus.com/inward/record.uri?eid=2-s2.0-84921325865&doi=10.1007%2fs11051-014-2807-2&partnerID=40&md5=28fa5347155e81b0a7db3b16b0770bf7.

28- E. Lechtman, N. Chattopadhyay, Z. Cai, S. Mashouf, R. Reilly, and J.P. Pignol, "Implications on clinical scenario of gold nanoparticle radiosensitization in regards to photon energy, nanoparticle size, concentration and location." *Phys. Med. Biol*, Vol. 56 (No. 15), pp. 4631-47, 8/7/2011 (2011).

29- L. Sancey *et al.*, "The use of theranostic gadolinium-based nanoprobes to improve radiotherapy efficacy." *Br. J. Radiol*, Vol. 87 (No. 1041), p. 20140134, 9/2014 (2014).

30- C. Lee, N.N. Cheng, R.A. Davidson, and T. Guo, "Geometry enhancement of nanoscale energy deposition by X-rays." Presented at the *J. Phys. Chem. C*

Journal of Physical Chemistry C, 2012, (2012). [Online]. Available: https://www.scopus.com/inward/record.uri?eid=2-s2.0-84861494114&doi=10.1021%2fjp210301q&partnerID=40&md5=cd4235079e6f19a2deb8a413e02fab59.